



A study of the \tilde{e} -system in SPS1a' at the ILC

Ryan Wilkinson, Durham University, UK

Supervisors: Dr. Mikael Berggren, Dr. Jenny List

September 8, 2011

Abstract

The e channel at the SUSY benchmark point SPS1a' from $e^+e^- \rightarrow \tilde{e}^+\tilde{e}^-$ has been studied using the full ILD detector simulation foreseen for the International Linear Collider. All accessible SUSY channels and Standard Model backgrounds were generated at a centre-of-mass energy $E_{CMS} = 500$ GeV with an integrated luminosity of 500 fb^{-1} delivered to the experiment and a beam polarisation $\mathcal{P}_{beam}(e^+, e^-) = (+0.8, -0.22)$. The masses of the \tilde{e}_R and $\tilde{\chi}_1^0$ were measured to be 123.9 ± 0.9 GeV and 98.8 ± 0.7 GeV respectively, with a reduced- χ^2 of 1.1, while the true values in SPS1a' are 125.3 GeV and 97.7 GeV.

Contents

1	Introduction	1
2	Spectrum Analysis	2
3	Mass Measurements	8
3.1	Signal Selection	8
3.2	Results	11
4	Summary & Conclusion	11

1 Introduction

This project builds on the ILC analysis of the τ -channel in SPS1a' [1], using a full detector simulation of SUSY processes (signal and background), all Standard Model (SM) backgrounds and ILC machine background. For a detailed description of the ILC detector, see [2]. The process $e^+e^- \rightarrow \tilde{e}^+\tilde{e}^- \rightarrow e^+\tilde{\chi}_1^0 e^-\tilde{\chi}_1^0$ (see Fig. 1) has been studied with the aim to extract the masses of the \tilde{e}_R and $\tilde{\chi}_1^0$ after a suitable signal selection and background reduction has been applied to the sample.

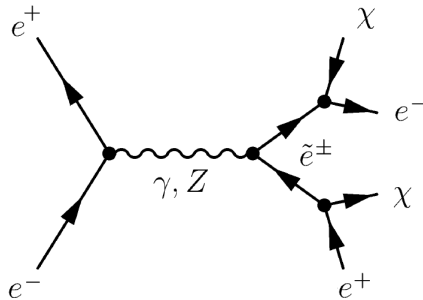


Figure 1: Feynman diagram of $e^+e^- \rightarrow \tilde{e}^+\tilde{e}^- \rightarrow e^+\tilde{\chi}_1^0 e^-\tilde{\chi}_1^0$.

The SUSY benchmark point SPS1a' is a pure mSUGRA/CMSSM model, characterised by the unification scale parameters: $M_{1/2} = 250$ GeV, $M_0 = 70$ GeV, $A_0 = -300$ GeV, $\tan\beta = 10$, and $\text{sign}(\mu) = +1$. It is compatible with the observations of WMAP, predicting SUSY particles just outside what is excluded by LEP and low-energy observations. The neutralino $\tilde{\chi}_1^0$ is the lightest SUSY particle (LSP) and in this scenario, would be a Dark Matter candidate. At $E_{CMS} = 500$ GeV, all sleptons would be produced, lighter bosinos up to $\tilde{\chi}_3^0$ and no squarks. There are a total of 13 distinct channels that would be observable below $E_{CMS} = 500$ GeV [3] and in this paper, the \tilde{e} channel will be investigated.

In SPS1a', the masses of the \tilde{e}_R and $\tilde{\chi}_1^0$ are 125.3 GeV and 97.7 GeV respectively, so that $\Delta(M) = 27.6$ GeV. The typical signature of $e^+e^- \rightarrow \tilde{e}^+\tilde{e}^-$ events is two e leptons with a minimal energy of $E_{e,min} = 6.6$ GeV and maximal energy of $E_{e,max} = 91.4$ GeV, plus a significant amount of missing momentum due to the escaping neutralinos. The masses of the \tilde{e}_R and $\tilde{\chi}_1^0$ can be obtained either from the decay kinematics or from the cross section. As $E_{e,min}$ is so low, the background from $\gamma\gamma \rightarrow ee$ events is overwhelming and measuring the lower endpoint becomes problematic.

The outline of the paper is as follows: In Sec. 2, the kinematics of the two-body decay are analysed. In Sec. 3.1, the method used to extract the \tilde{e} signal is outlined by first identifying the significant differences between the signal and various backgrounds and then presenting the consequent signal selection. In Sec. 3.2, a description of the method used to determine the endpoints of the e spectrum and the main results of the project are given. The paper is concluded in Sec. 4.

2 Spectrum Analysis

We are interested in the decay $\tilde{e} \rightarrow e + \tilde{\chi}_1^0$. The Feynman diagram for the process is shown in Fig. 1. In order to extract the masses of the \tilde{e}_R and $\tilde{\chi}_1^0$, we need to relate $M_{\tilde{e}_R}$ and $M_{\tilde{\chi}_1^0}$ to the endpoints of the e energy spectrum, $E_{e,min}$ and $E_{e,max}$.

In the **rest frame of the \tilde{e} (S')**, assuming the e travels isotropically in 3-dim. space and neglecting the e mass,

$$P_{\tilde{e}}^{\mu'} = \left(M_{\tilde{e}}, 0, 0, 0 \right), \quad (1)$$

$$P_e^{\mu'} = \left(E'_e, E'_e \sin(\theta') \cos(\phi'), E'_e \sin(\theta') \sin(\phi'), E'_e \cos(\theta') \right). \quad (2)$$

In the **centre of mass frame (S)**, with E_{CM} as the total energy of the system,

$$P_{\tilde{e}}^{\mu} = \left(\frac{E_{CM}}{2}, 0, 0, \sqrt{\left(\frac{E_{CM}}{2} \right)^2 - M_{\tilde{e}}^2} \right), \quad (3)$$

$$P_e^{\mu} = \left(E_e, E_e \sin(\theta) \cos(\phi), E_e \sin(\theta) \sin(\phi), E_e \cos(\theta) \right). \quad (4)$$

The Lorentz transformation matrix for a boost in the z -direction is

$$\Lambda^{\mu}_{\nu} = \begin{pmatrix} \gamma & 0 & 0 & -\gamma\beta \\ 0 & 1 & 0 & 0 \\ 0 & 0 & 1 & 0 \\ -\gamma\beta & 0 & 0 & \gamma \end{pmatrix}. \quad (5)$$

Assuming the \tilde{e} is moving in the z -direction in S, we can relate Eqs. (1) and (3) by the boost matrix in Eq. (5) to obtain

$$\gamma = \frac{E_{CM}}{2M_{\tilde{e}}}, \quad -\gamma\beta = \sqrt{\left(\frac{E_{CM}}{2M_{\tilde{e}}} \right)^2 - 1}. \quad (6)$$

For e , relating Eqs. (2) and (4),

$$E_e = \gamma E'_e (1 + \beta \cos(\theta')). \quad (7)$$

From kinematic considerations, we also know that

$$E'_e = \frac{M_{\tilde{e}}^2 - M_{\tilde{\chi}_1^0}^2}{2M_{\tilde{e}}}. \quad (8)$$

Substituting Eqs. (6) and (8) into Eq. (7),

$$E_e(\theta') = \frac{E_{\text{CM}}}{4} \left[1 - \left(\frac{M_{\tilde{\chi}_1^0}}{M_{\tilde{e}}} \right)^2 \right] \left[1 + \sqrt{1 - \left(\frac{2M_{\tilde{e}}}{E_{\text{CM}}} \right)^2} \cos(\theta') \right]. \quad (9)$$

Similarly, we find that

$$p_{e,z}(\theta') = \frac{E_{\text{CM}}}{4} \left[1 - \left(\frac{M_{\tilde{\chi}_1^0}}{M_{\tilde{e}}} \right)^2 \right] \left[\cos(\theta') + \sqrt{1 - \left(\frac{2M_{\tilde{e}}}{E_{\text{CM}}} \right)^2} \right]. \quad (10)$$

The maximal and minimal energies will be for $\theta' = 0$ and $\theta' = \pi$ respectively i.e.

$$E_{e,(\min)} = \frac{E_{\text{CM}}}{4} \left[1 - \left(\frac{M_{\tilde{\chi}_1^0}}{M_{\tilde{e}}} \right)^2 \right] \left[1 - \sqrt{1 - \left(\frac{2M_{\tilde{e}}}{E_{\text{CM}}} \right)^2} \right]. \quad (11)$$

Assuming a uniform distribution, the width (ΔE_e) and mean (\bar{E}_e) of the e energy spectrum are then

$$\Delta E_e = \frac{E_{\text{CM}}}{2} \left[1 - \left(\frac{M_{\tilde{\chi}_1^0}}{M_{\tilde{e}}} \right)^2 \right] \left[\sqrt{1 - \left(\frac{2M_{\tilde{e}}}{E_{\text{CM}}} \right)^2} \right], \quad \bar{E}_e = \frac{E_{\text{CM}}}{4} \left[1 - \left(\frac{M_{\tilde{\chi}_1^0}}{M_{\tilde{e}}} \right)^2 \right]. \quad (12)$$

We can invert Eq. (12) to extract the masses of the \tilde{e} and $\tilde{\chi}_1^0$,

$$M_{\tilde{e}} = \frac{E_{\text{CM}}}{2} \sqrt{1 - \left(\frac{\Delta E_e}{2\bar{E}_e} \right)^2}, \quad M_{\tilde{\chi}_1^0} = M_{\tilde{e}} \sqrt{1 - \frac{4\bar{E}_e}{E_{\text{CM}}}}. \quad (13)$$

Assuming the e is emitted isotropically in S' , we know from geometrical considerations that θ' has a sinusoidal distribution i.e.

$$\theta'(x) = \sin(x), \quad (14)$$

so we can combine Eq. (14) with Eq. (9) to determine the energy distribution of the e . We have that

$$\theta'(x) = \sin(x) \equiv f(x), \quad E_e(\theta') = \bar{E}_e + \Delta E_e \cdot \cos(\theta') \equiv g(\theta'), \quad (15)$$

By definition,

$$F_{\theta'}(x) \equiv P(\theta' \leq x), \quad (16)$$

and so

$$F_E(x) \equiv P(E \leq x) = P(g(\theta') \leq x) = P(\theta' \leq g^{-1}(x)) = F_{\theta'}(g^{-1}(x)). \quad (17)$$

Since we know that

$$f_{\theta'}(x) = \frac{d}{dx} F_{\theta'}(x) , \quad (18)$$

and

$$g^{-1}(x) = \arccos \left[\frac{(x - \bar{E}_e)}{\Delta E_e} \right] , \quad (19)$$

we can write

$$F_E(x) = \left[\frac{(x - \bar{E}_e)}{\Delta E_e} \right] . \quad (20)$$

Differentiating with respect to x ,

$$f(E_e) = \frac{1}{\Delta E_e} . \quad (21)$$

Eq. (21) must integrate to unity so we get a box-distribution centred around \bar{E}_e ,

$$f(E_e) = \begin{cases} \frac{1}{\Delta E_e} & (\bar{E}_e - \frac{\Delta E_e}{2} \leq E_e \leq \bar{E}_e + \frac{\Delta E_e}{2}) , \\ 0 & \text{else} . \end{cases} \quad (22)$$

However, the actual e energy spectrum is distorted from a simple box distribution (see Figs. 6, 7). There are two reasons for this:

1. Although the total energy in the centre of mass frame, E_{CM} , is fixed, the individual beam energies will vary around $E_{\text{CM}}/2$. Therefore, the beam momenta will differ and the **lab frame (S*)** will not coincide with the CM frame (S).
2. Distortion from the detector. The signal is measured with greater precision at low energies and there is a bias towards a smaller mean from the calorimeter. However, this effect will be negligible compared to (1).

To examine the effect of (1) on the energy spectrum, we can apply a second boost matrix such that the combined 4-momentum of the two beams satisfies

$$\begin{bmatrix} E_{\text{lab}} \\ 0 \\ 0 \\ z \end{bmatrix} = \begin{bmatrix} \gamma & 0 & 0 & -\gamma\beta \\ 0 & 1 & 0 & 0 \\ 0 & 0 & 1 & 0 \\ -\gamma\beta & 0 & 0 & \gamma \end{bmatrix} \begin{bmatrix} E_{\text{CM}} \\ 0 \\ 0 \\ 0 \end{bmatrix} , \quad (23)$$

where $z > 0$ is the additional longitudinal momentum due to the non-coinciding inertial frames S and S*. We assume that the total energy in S*, E_{lab} , is known.

From Eq. (23), we see that

$$\gamma = \frac{E_{\text{lab}}}{E_{\text{CM}}} , \quad -\gamma\beta = \frac{z}{E_{\text{CM}}} , \quad (24)$$

and due to Lorentz invariance,

$$E_{\text{CM}} = \sqrt{E_{\text{lab}}^2 - z^2} = E_{\text{lab}} \sqrt{1 - \left(\frac{z}{E_{\text{lab}}}\right)^2}. \quad (25)$$

Applying the boost matrix in Eq. (23) to the 4-momentum of e in S,

$$E_e^* = \gamma E_e - \gamma \beta p_{e,z}. \quad (26)$$

Substituting the expressions for E_e (Eq. (9)), $p_{e,z}$ (Eq. (10)) and γ and $-\gamma\beta$ (Eq. (24)) into Eq. (26),

$$\begin{aligned} E_e^*(\theta', z) &= \frac{E_{\text{lab}}}{4} \left[1 - \left(\frac{M_{\tilde{\chi}_1^0}}{M_{\tilde{e}}} \right)^2 \right] \left[1 - \left(\frac{z}{E_{\text{lab}}} \right)^2 \right]^{-\frac{1}{2}} \\ &\times \left\{ \left[1 + \sqrt{1 - \left(\frac{2M_{\tilde{e}}}{E_{\text{lab}}} \right)^2} \cos(\theta') \right] + \frac{z}{E_{\text{lab}}} \left[\cos(\theta') + \sqrt{1 - \left(\frac{2M_{\tilde{e}}}{E_{\text{lab}}} \right)^2} \right] \right\} \end{aligned} \quad (27)$$

Setting $z = 0$ so that $E_{\text{lab}} = E_{\text{CM}}$, we recover the expression for E_e in S (Eq. (9)). We can also determine the maximal and minimal energies by setting $\theta' = 0$ and $\theta' = \pi$ respectively,

$$\begin{aligned} E_{e, (min)}^*(z) &= \frac{E_{\text{lab}}}{4} \left[1 - \left(\frac{M_{\tilde{\chi}_1^0}}{M_{\tilde{e}}} \right)^2 \right] \left[1 \frac{-}{(+)} \sqrt{1 - \left(\frac{2M_{\tilde{e}}}{E_{\text{lab}}} \right)^2} \right] \\ &\times \left[1 - \left(\frac{z}{E_{\text{lab}}} \right)^2 \right]^{-\frac{1}{2}} \left[1 \frac{-}{(+)} \frac{z}{E_{\text{lab}}} \right] \\ &= E_{e, (min)} \times \left[1 - \left(\frac{z}{E_{\text{lab}}} \right)^2 \right]^{-\frac{1}{2}} \left[1 \frac{-}{(+)} \frac{z}{E_{\text{lab}}} \right]. \end{aligned} \quad (28)$$

A greater value of z results in a wider distribution. However, since z will usually be much smaller than E_{lab} , we would not expect a significant distortion to the spectrum due to the variation of the momenta of the two beams.

Assuming the additional momentum z is constant, we can write that

$$E_e^*(\theta') = A(\bar{E}_e + \Delta E_e \cdot \cos(\theta')) + B(\bar{E}_e \cos(\theta') + \Delta E_e) \equiv g(\theta'), \quad (29)$$

where A and B are the constants

$$A = \left[1 - \left(\frac{z}{E_{\text{lab}}} \right)^2 \right]^{-\frac{1}{2}}, \quad B = \frac{z}{E_{\text{lab}}} \left[1 - \left(\frac{z}{E_{\text{lab}}} \right)^2 \right]^{-\frac{1}{2}}. \quad (30)$$

The inverse

$$g^{-1}(x) = \arccos \left[\frac{x - A\bar{E}_e - B \cdot \Delta E_e}{A \cdot \Delta E_e - B\bar{E}_e} \right]. \quad (31)$$

Following the same procedure as before, we find that

$$f(E_e^*) = \frac{1}{A \cdot \Delta E_e - B\bar{E}_e}. \quad (32)$$

Thus for constant z , the e energy distribution is still uniform. Note that if $z = 0$, $A = 1$ and $B = 0$ so we recover the box distribution for $S^* = S$ (Eq. (21)).

For small z , we can make the first order Taylor approximation, $[1 + (z/E_{\text{lab}})^2]^{-1/2} \simeq 1$. Eq. (27) simplifies to

$$E_e^*(\theta', z) \simeq E_e(\theta) + \frac{z}{4} \left[1 - \left(\frac{M_{\tilde{\chi}_1^0}}{M_{\tilde{e}}} \right)^2 \right] \left[\cos(\theta') + \sqrt{1 - \left(\frac{2M_{\tilde{e}}}{E_{\text{lab}}} \right)^2} \right], \quad (33)$$

and again taking only first order terms,

$$\begin{aligned} [E_e^*(\theta', z)]^2 &\simeq [E_e(\theta)]^2 + \left\{ \frac{z \cdot E_{\text{lab}}}{8} \left[1 - \left(\frac{M_{\tilde{\chi}_1^0}}{M_{\tilde{e}}} \right)^2 \right]^2 \right. \\ &\quad \times \left. \left[\cos(\theta') + \sqrt{1 - \left(\frac{2M_{\tilde{e}}}{E_{\text{lab}}} \right)^2} \right] \left[1 + \sqrt{1 - \left(\frac{2M_{\tilde{e}}}{E_{\text{lab}}} \right)^2} \cos(\theta') \right] \right\}. \end{aligned} \quad (34)$$

Now we assume that z takes values from 0 to z_{max} . In S^* , we require that the total energy of the two beams is E_{lab} and the difference is z (we assume that E_{lab} is fixed). So, neglecting the beam spectra, the energies of the two beams would be

$$E_{e,1}^* = \frac{1}{2}(E_{\text{lab}} - z), \quad E_{e,2}^* = \frac{1}{2}(E_{\text{lab}} + z). \quad (35)$$

To a reasonable approximation, the beam spectra will be Gaussian, with mean values given by Eq. (35). To see the effect of the beam spectra on the e energy distribution, we can perform the integration

$$\int_0^{z_{\text{max}}} A \exp \left[-\frac{(E_e - \frac{1}{2}(E_{\text{lab}} - z))^2}{c_1^2} \right] + B \exp \left[-\frac{(E_e - \frac{1}{2}(E_{\text{lab}} + z))^2}{c_2^2} \right] dz, \quad (36)$$

where A , B , c_1 and c_2 are constants that depend on the shape of the Gaussian distributions. Performing the integration, we find

$$f(E_e) = a_1 \operatorname{erf} \left[\frac{E_e + b_1}{c_1} \right] - a_2 \operatorname{erf} \left[\frac{E_e - b_2}{c_2} \right] + a_3, \quad (37)$$

where a_1 , a_2 , a_3 , b_1 and b_2 are constants and $\operatorname{erf}(x)$ is the (Gauss) error function.

Fig. 2 shows the effect of a Gaussian beam spectrum on the e energy distribution. If the two beam spectra are different, it is reasonable to suggest that this is a cause of the asymmetry in Figs. 6 and 7, and the deviation from a simple box distribution. However, the beam spectrum is not simply a Gaussian but has a tail to lower energies. Further work will be needed to see the effect that this has on the energy spectrum.

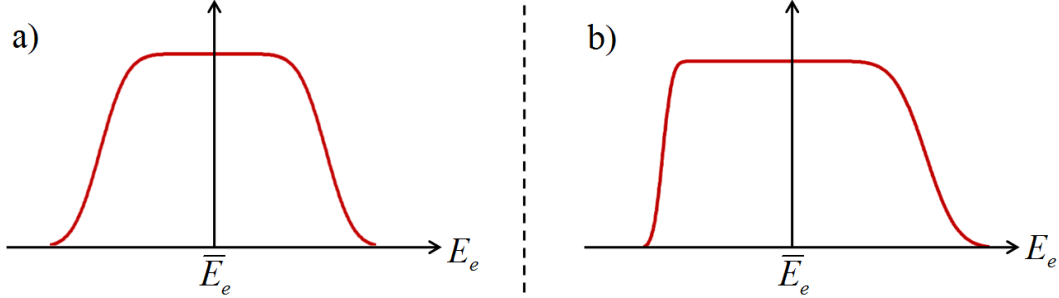


Figure 2: The e energy distribution assuming a Gaussian beam spectrum when a) the two Gaussians are identical, b) the two Gaussians are different ($c_1 \neq c_2$).

Additionally, we have assumed that the total energy, E_{lab} , is constant but in reality, this will also vary. Using Eq. (28), we can plot the dependence of the endpoints on E_{lab} (see Fig. 3). For energies close to E_{lab} , the upper endpoint has an almost linear dependence, while the lower endpoint varies only slightly. Therefore, this also contributes to the distinctive shape of the energy spectrum. Further investigation will be needed to show the relative contribution to the distortion from other sources such as beamstrahlung.

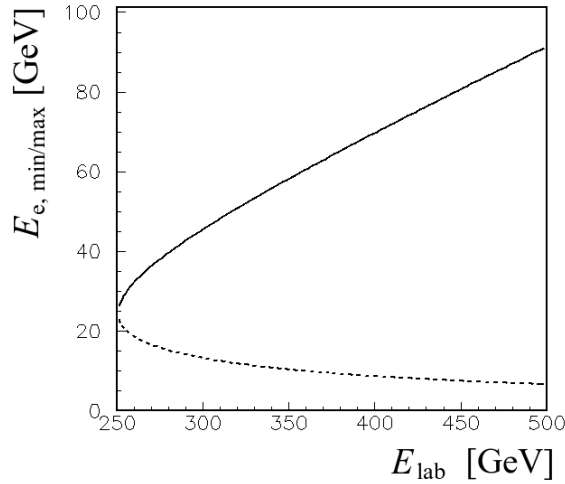


Figure 3: The upper endpoint (solid line) and lower endpoint (dashed line) as a function of E_{lab} , where E_{lab} takes values from the threshold energy $E_{lab} = 2M_{\tilde{e}_R}$ to the maximum energy of 500 GeV.

3 Mass Measurements

3.1 Signal Selection

Before we could accurately determine the masses of the \tilde{e}_R and $\tilde{\chi}_1^0$, it was necessary to reduce beam-beam and $\gamma\gamma$ backgrounds, find e candidates and select selectron-like topology. The signal selection was developed from that of the stau analysis [1]. Note that for this study, $E_{CMS} = 500$ GeV with an integrated luminosity of 500 fb^{-1} and a polarisation $\mathcal{P}_{beam}(e^+, e^-) = (+0.8, -0.22)$. The key characteristics of \tilde{e} production and decay, which distinguish it from the background are:

- only two e leptons in the final state
- large missing energy and momentum
- high acollinearity, which little correlation to the energy of the e decay products
- central production
- no forward-background asymmetry.

Before selection, the signal was dominated by the $\gamma\gamma$ background and since we used the entire spectrum for mass measurements, the SUSY background also needed to be addressed. At this stage, the number of events were: 3.32×10^5 (signal), 1.64×10^9 (SM background) and 9.57×10^4 (SUSY background).

Stage 1: Events compatible with the \tilde{e} topology were selected requiring:

- exactly two jets
- less than 10 charged particle candidates
- vanishing total charge, with charge of each jet = ± 1
- invariant jet masses $M_{jet} < 2.5$ GeV for both jets
- a total visible energy $E_{vis} < 170$ GeV (looser than for the $\tilde{\tau}$ analysis)
- a missing mass $M_{miss} > 250$ GeV
- no particles with momentum above 180 GeV,

where M_{miss} is the invariant mass of the invisible system, determined by the difference between the initial e^+e^- system and the visible system. It was suggested that the cut on the visible energy be adjusted to $E_{vis} < 144$ GeV, which increases the signal to background ratio significantly; however, the effect on the shape of the spectrum was too severe. After this initial selection, the number of events were: 2.88×10^5 (signal), 6.50×10^8 (SM background) and 6.66×10^4 (SUSY background).

Stage 2: The major characteristics of the $\gamma\gamma$ background are two highly energetic electrons at low angles and a system of low energy and mass. We also have remnants escaping the detector through the incoming or outgoing beampipe. To reduce the $\gamma\gamma$ background, the following two cuts were applied:

- If $\phi_{pt,miss} < 30^\circ$, then $\rho_{\perp,miss} > 8$ GeV
- $2\sqrt{\rho_{\perp}} > (2.7 \sin \Phi_{acop} + 1.8)$ GeV,

where $\phi_{pt,miss}$ is the azimuthal angle of the missing momentum and Φ_{acop} is the angle between the two jets projected to the plane perpendicular to the beam axis. The variable ρ_{\perp} is the scalar sum of the transverse momenta of the jets with respect to the thrust axis, in the projection perpendicular to the beam. For further details on these cuts, see [1]. At this stage, the number of events were: 2.70×10^5 (signal), 8.85×10^5 (SM background) and 3.30×10^4 (SUSY background).

Stage 3: To further reduce the background, the following cuts were made:

- $21 \text{ GeV} < (E_{jet1} + E_{jet2}) \sin \Phi_{acol} < 105 \text{ GeV}$ (see Fig. 4)
- $|\cos \theta_{pt,miss}| < 0.95$ (see Fig. 5)
- $E_{had,jet} < 0.015 E_{jet}$, $E_{elec,jet} > 0.9 E_{jet}$,

where the final cut selects events with large electromagnetic and small hadronic contributions. After this final selection, the number of events remaining were: 8.79×10^4 (signal), 2.32×10^3 (SM background) and 1.53×10^3 (SUSY background), with $\text{Signal}/(\text{Background})^{1/2} \simeq 1400$ (see Table 1 for a summary).

Stage	Signal	SM background	SUSY background
Before cuts	3.32×10^5	1.64×10^9	9.57×10^4
1	2.88×10^5	6.50×10^8	6.66×10^4
2	2.70×10^5	8.85×10^5	3.30×10^4
3	8.79×10^4	2.32×10^3	1.53×10^3

Table 1: The number of counts at each stage of the signal selection process.

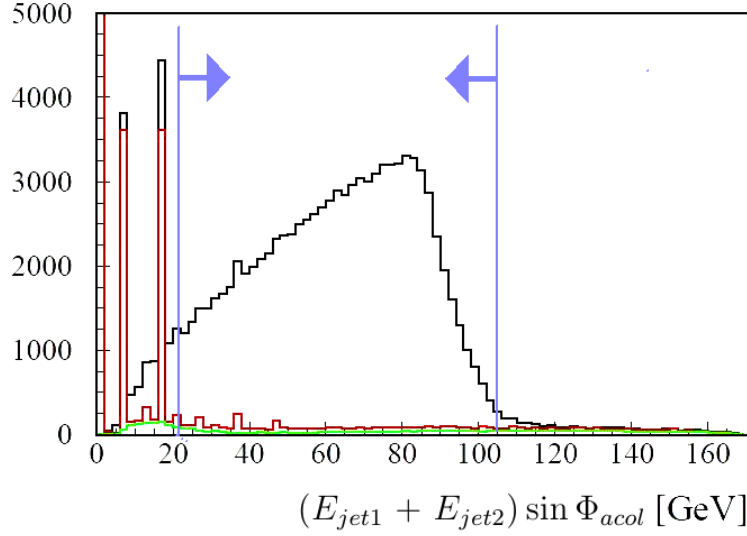


Figure 4: The distribution of the sum of the jet energies multiplied by the sine of the acollinearity angle, showing the signal (black histogram), SM background (red) and SUSY background (green). The cut, given by the blue lines, corresponds to $21 \text{ GeV} < (E_{jet1} + E_{jet2}) \sin \Phi_{acol} < 105 \text{ GeV}$. The selected events are enclosed by the lines.

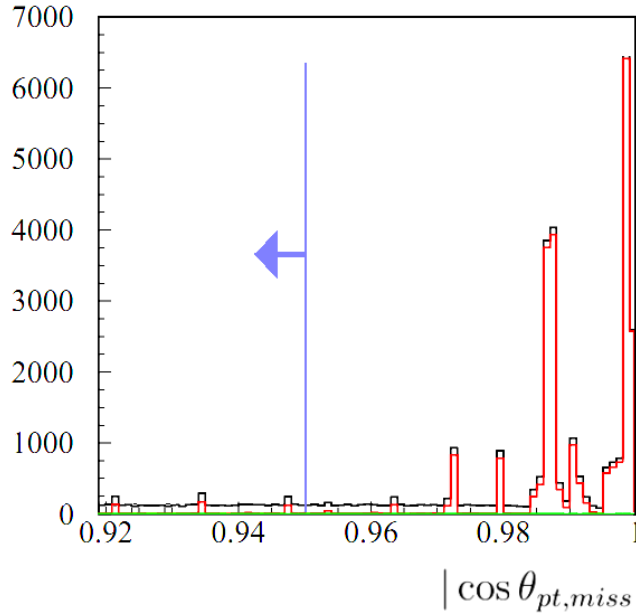


Figure 5: The distribution of the absolute value of the cosine of the missing momentum angle, showing the signal (black histogram), SM background (red) and SUSY background (green). The cut, given by the blue line, corresponds to $|\cos \theta_{pt,miss}| < 0.95$. The selected events lie to the left of the line.

3.2 Results

Fig. 6 shows the electron energy spectrum at the generator level, before the addition of the SM and SUSY backgrounds. Fig. 7 shows the spectrum after the signal selection discussed in Sec. 3.1 had been applied to the sample. The overall shape of the spectrum is maintained, however the endpoints are distorted by both the cuts and the beam spectrum. Note again that $E_{CMS} = 500$ GeV, $\int L dt = 500 \text{ fb}^{-1}$ and $\mathcal{P}_{beam}(e^+, e^-) = (+0.8, -0.22)$.

For a uniform distribution, the standard deviation $\sigma = \text{width}/\sqrt{12}$. We can use the width (ΔE_e) and mean (\bar{E}_e) to determine the masses of the \tilde{e}_R and $\tilde{\chi}_1^0$ from Eq. (13). Doing so gives $M_{\tilde{e}_R} = 118.5 \pm 0.5$ GeV and $M_{\tilde{\chi}_1^0} = 95.2 \pm 0.4$ GeV (the actual values in SPS1a' are $M_{\tilde{e}_R} = 125.3$ GeV and $M_{\tilde{\chi}_1^0} = 97.7$ GeV). Considering only the signal, we find improved estimates of $M_{\tilde{e}_R} = 119.9 \pm 0.5$ GeV and $M_{\tilde{\chi}_1^0} = 96.3 \pm 0.4$ GeV. However, this analysis assumes that the distribution is uniform; the effect of the beam spectrum is to skew the masses to lower values.

In order to overcome this, the sum of the two jet energies, $E_{jet1} + E_{jet2}$, was considered (see Fig. 8). Because we are essentially adding two box distributions, the overall shape of the spectrum is triangular. A fit was added to the plot (see Fig. 9 for details) which returns the masses directly, using the expressions in Eqs. (12) and (13). Two constraints were applied to the fit: 1) The area contained by the triangle should equal the combined area of the signal, SM background and SUSY background histograms, 2) the gradients of the fit either side of the mean should be equal and opposite.

Applying the fit to the entire spectrum gives us rather high values: $M_{\tilde{e}_R} = 144.9 \pm 0.5$ GeV and $M_{\tilde{\chi}_1^0} = 115.1 \pm 0.4$ GeV. However, since we know that the endpoints are greatly affected by the beam spectrum, a second fit was taken in the range 40 - 150 GeV (as shown in Fig. 8), ensuring that there was less bias in the reconstructed masses. Doing so gives values of $M_{\tilde{e}_R} = 123.9 \pm 0.9$ GeV and $M_{\tilde{\chi}_1^0} = 98.8 \pm 0.7$ GeV, which differ from the actual values in SPS1a' by two standard deviations.

Lastly, with the masses from the triangle fit, we can calculate the endpoints of the spectrum using Eq. (11). We find that $E_{e,min} = 5.97 \pm 0.07$ GeV and $E_{e,max} = 84.9 \pm 0.9$ GeV (the expected values in SPS1a' are $E_{e,min} = 6.60$ GeV and $E_{e,max} = 91.4$ GeV). It should be noted that for all the fits applied, the reduced- χ^2 values were 1.1.

4 Summary & Conclusion

A study of the \tilde{e} channel in SPS1a' based on a full simulation of the ILD detector at the ILC has been presented. All known SUSY, SM and machine related backgrounds were included in the simulation, and we assumed that $E_{CMS} = 500$ GeV, the integrated luminosity = 500 fb^{-1} and the polarisation $\mathcal{P}_{beam}(e^+, e^-) = (+0.8, -0.22)$.

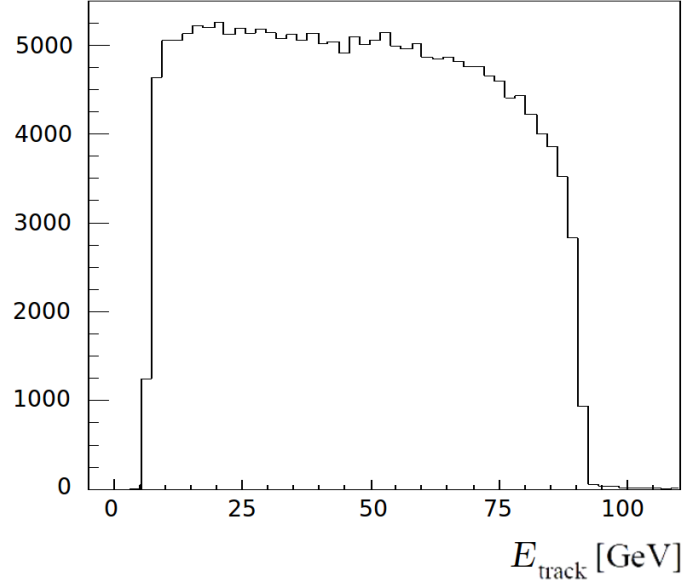


Figure 6: The electron jet energy spectrum of events at the generator level, before the background is added. The mean energy is 49.0 GeV with a standard deviation of 24.5 GeV.

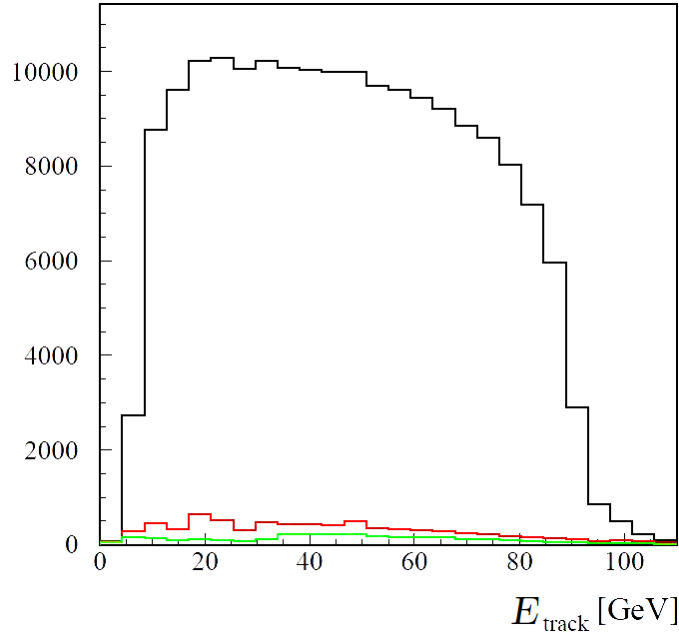


Figure 7: The electron jet energy spectrum of events selected in the \tilde{e} analysis, showing the signal (black histogram), SM background (red) and SUSY background (green). The mean energy is 47.2 GeV with a standard deviation of 23.6 GeV.

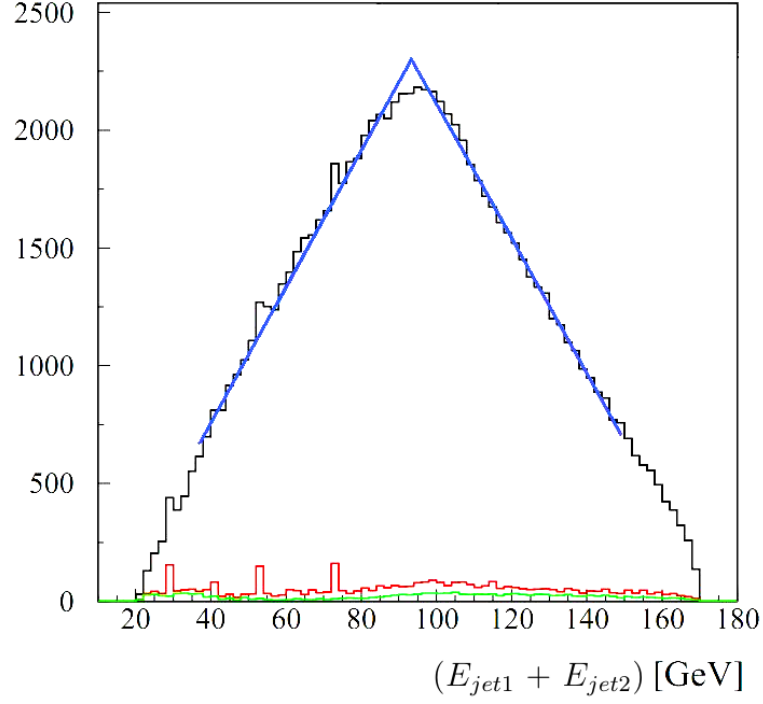


Figure 8: The spectrum of the sum of jet energies, showing the signal (black histogram), SM background (red) and SUSY background (green). A triangular fit to the sample from 40 GeV to 150 GeV is indicated by the blue line.

```

*PAR(1): selectron mass, PAR(2): LSP mass

*PAR(1) = 250 * SQRT(1-(width/(2*mean))**2)
*PAR(2) = PAR(1) * SQRT(1-(mean/125))

REAL FUNCTION TRIMASS(X)
COMMON/PAWPAR/PAR(2)

area = 0.8862*(10**5)
mean = 250*(1-(PAR(2)/PAR(1))**2)
width = 2*mean*SQRT(1-(PAR(1)/250)**2)
peak = (2*area)/width
gradient = (peak**2)/(area)

IF (X.LT.mean) THEN
    TRIMASS = peak-(gradient*(mean-X))
ELSE
    TRIMASS = peak-(gradient*(X-mean))
ENDIF
END

```

Figure 9: The function used to fit a triangular shape to the combined jet energy spectrum (Fig. 8) and directly return the masses of the \tilde{e}_R and $\tilde{\chi}_1^0$.

The results from the study of the electron energy spectra were:

$$\begin{aligned} E_{e,min} &= 5.97 \pm 0.07 \text{ GeV (6.60 GeV)} & E_{e,max} &= 84.9 \pm 0.9 \text{ GeV (91.4 GeV)} \\ M_{\tilde{e}_R} &= 123.9 \pm 0.9 \text{ GeV (125.3 GeV)} & M_{\tilde{\chi}_1^0} &= 98.8 \pm 0.7 \text{ GeV (97.7 GeV)} \end{aligned}$$

where the actual values in SPS1a' are shown in brackets. The reduced- χ^2 value of the fit was 1.1. The measured masses differ from the actual values in SPS1a' by 2 standard deviations. This is most likely due to the limitations of the signal selection, which unfortunately alter the shape of the distribution, and distortions from the beam spectrum.

A more thorough analysis of the cuts combined with larger Monte Carlo statistics would inevitably improve these estimations. It should be noted that the uncertainties given here are the optimum; however, achieving a value for $M_{\tilde{\chi}_1^0}$ with an uncertainty of less than 1 % by looking at only one channel is encouraging and more work into this area could prove to be very beneficial.

This paper has only considered \tilde{e} -pair production; the other open channels were considered as SUSY background. However, the $\tilde{\tau}$ channel has been studied in [1], where it was found that $M_{\tilde{\chi}_1^0}$ could be determined with a relative error of 1.7 % (assuming a known $\tilde{\tau}$ mixing angle).

With regards to future analysis, rather than looking at the decay kinematics, the cross section could be used to determine the masses. Additionally, many more channels could be investigated to sharpen the estimations, with different values for E_{CMS} and the polarisation (it has been suggested in [1], that for many processes, running the accelerator at $E_{CMS} = 500 \text{ GeV}$ may not be optimal).

Finally, we have shown the effect of a simple Gaussian beam spectrum on the e energy distribution, however, a deeper study into the exact shape of the beam spectrum and an investigation into other sources of distortion such as beamstrahlung would be advantageous.

I would like to thank my supervisors Dr. M. Berggren and Dr. J. List for their invaluable assistance during my time in the FLC group. The project has been a interesting and useful experience, and I am extremely grateful for the opportunity to work at DESY.

References

- [1] *P. Bechtle & al.*, arXiv:0908:0876 (2009), <http://arxiv.org/ps/0908.0876>.
- [2] ILD Concept Group, *The International Large Detector – Letter of Intent*, (DESY-09-087), <http://www.ilcild.org/documents/ild-letter-of-intent/LOI.pdf>.
- [3] *M. Berggren*, arXiv:1007.3019 (2010), <http://arxiv.org/ps/1007.3019>.